nature nanotechnology

LETTERS

PUBLISHED ONLINE: 8 AUGUST 2010 | DOI: 10.1038/NNANO.2010.154

Very large magnetoresistance in graphene nanoribbons

Jingwei Bai[1†], Rui Cheng[1†], Faxian Xiu[2], Lei Liao[3], Minsheng Wang[2], Alexandros Shailos[4], Kang L. Wang[2,4], Yu Huang[1,4]* and Xiangfeng Duan[3,4]*

Graphene has unique electronic properties[1,2], and graphene nanoribbons are of particular interest because they exhibit a conduction bandgap that arises due to size confinement and edge effects[3–11]. Theoretical studies have suggested that graphene nanoribbons could have interesting magneto-electronic properties, with a very large predicted magnetoresistance[4,12–20]. Here, we report the experimental observation of a significant enhancement in the conductance of a graphene nanoribbon field-effect transistor by a perpendicular magnetic field. A negative magnetoresistance of nearly 100% was observed at low temperatures, with over 50% magnetoresistance remaining at room temperature. This magnetoresistance can be tuned by varying the gate or source–drain bias. We also find that the charge transport in the nanoribbons is not significantly modified by an in-plane magnetic field. The large observed values of magnetoresistance may be attributed to the reduction of quantum confinement through the formation of cyclotron orbits and the delocalization effect under the perpendicular magnetic field[15–20].

Graphene nanoribbon field-effect transistors (FETs) were fabricated using SiO_2 nanowires as physical etching masks (see Methods for details)[11]. A typical device has a narrow graphene nanoribbon as a semiconducting channel, with the channel width determined by the diameter of the nanowire mask and its length defined by electron-beam lithography. Source and drain contacts were formed by electron-beam evaporation of a titanium/gold film covering graphene blocks. A highly p-type doped silicon wafer was used as the back-gate, with a 300-nm-thick SiO_2 layer as the gate dielectric (Fig. 1). Unlike graphene nanoribbons defined by electron-beam lithography, in which polymeric resist residue may heavily dope the nanoribbons, resulting in a large positive shift of the charge neutrality point[21], the graphene nanoribbons obtained with the present method exhibit a relatively neat performance, with charge neutrality points typically in the range 0–5 V in the back-gate configuration[21].

The electrical transport characteristics of the graphene nanoribbon devices were determined at 1.6 K unless otherwise mentioned. In Fig. 2a, the black line indicates a differential conductance with respect to the gate voltage for a typical nanoribbon device with a channel width of ~15 nm and length of 800 nm. The curve suggests a strong suppression of conduction in this relatively long device, with a transport gap in the gate region of 0.4–6.6 V. Figure 2b shows differential conductance as a function of both the gate voltage V_g and the source–drain bias V_{sd}; a diamond-like characteristic of suppressed conductance consisting of a number of sub-diamonds is clearly seen. Note that smaller diamonds are also observed away from the main transport gap region (Fig. 2b), indicating that charge transport in the present device may be described by the model of multiple graphene quantum dots in series along the nanoribbon[22–26]. The formation of a quantum dot structure in the nanoribbons may be attributed to edge roughness or local potential variation[5,8,22,23].

We also performed magneto-transport measurements under a magnetic field up to 8 T normal to the device plane. Previous magnetoresistance studies of large graphene flakes have shown a non-saturated positive magnetoresistance near the minimum conductance point, representing carrier transport through inhomogeneously distributed electron and hole puddles of equal mobility[27,28]. In contrast, our graphene nanoribbon device exhibits a very large negative magnetoresistance that is highly dependent on the exact gate voltage and source–drain bias. Upon applying a magnetic field, the overall conductance increases dramatically, with a much reduced transport gap in the gate sweep (red curve in Fig. 2a). Near the edge of the original transport gap (back-gate voltage (V_g) range ~0.4–1.9 V and ~4.6–6.6 V), the differential conductance is essentially switched on from a completely off state upon applying the magnetic field (8 T), with the differential conductance increasing by a factor of 1,000 or more. On the other hand, the average conductance rises by a factor of ~2–4 when the device is gated far away from the transport gap region ($V_g < 0.4$ V or $V_g > 6.6$ V). This phenomenon is more evident in the two-dimensional differential conductance plots shown in Fig. 2b–d. The overall diamond of suppressed conductance shrinks significantly in both the gate and source–drain bias directions, and those sub-diamonds at the edge of the transport gap region become so conductive that the transport gap reduces to 1.9–4.6 V in the gate sweep at 8 T.

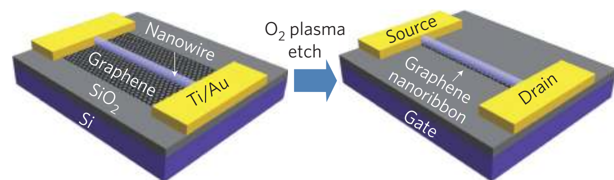

Figure 1 | Schematic of fabrication of a graphene nanoribbon FET using a nanowire as a physical etching mask. The device was fabricated on a heavily doped silicon substrate with a 300-nm-thick layer of SiO_2 as the gate dielectric. Electron-beam lithography was used to define and electron-beam evaporation to deposit a titanium/gold (7 nm/90 nm) film on a graphene block to be used as the source and drain electrodes.

[1]Department of Materials Science and Engineering, University of California, Los Angeles, California 90095, USA, [2]Department of Electrical Engineering, University of California, Los Angeles, California 90095, USA, [3]Department of Chemistry and Biochemistry, University of California, Los Angeles, California 90095, USA, [4]California NanoSystems Institute, University of California, Los Angeles, California 90095, USA; †These authors contributed equally to this work. *e-mail: xduan@chem.ucla.edu; yhuang@seas.ucla.edu

© 2010 Macmillan Publishers Limited. All rights reserved.

NATURE NANOTECHNOLOGY DOI: 10.1038/NNANO.2010.154

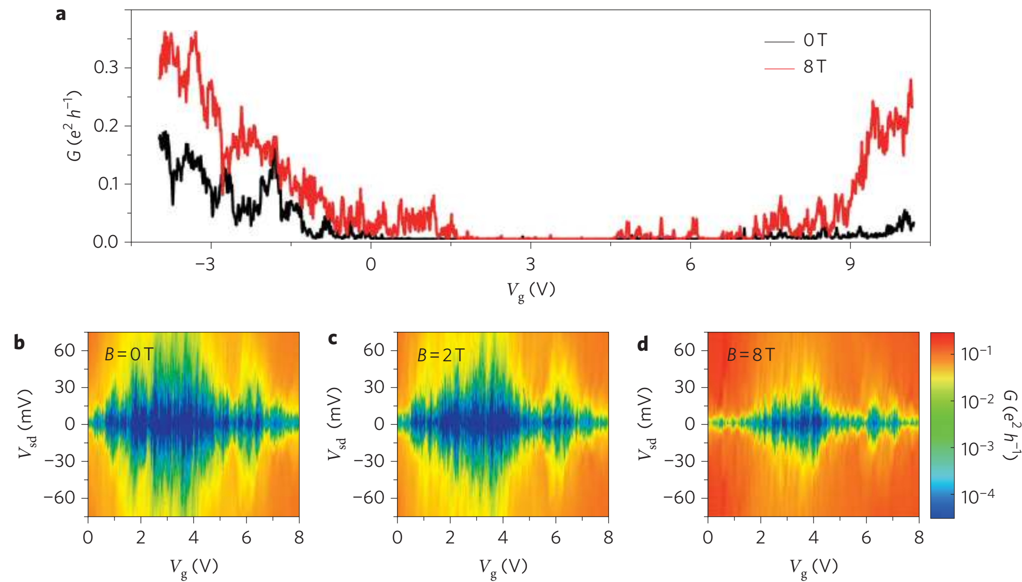

Figure 2 | Electrical transport measurements of a graphene nanoribbon FET with a channel width of ∼15 nm and length of 800 nm. a, Differential conductance versus gate voltage with a magnetic field of 0 T (black) and 8 T (red) normal to the device plane. Measurements were carried out at 1.6 K. **b–d**, Differential conductance as a function of source–drain bias and back-gate voltage under applied magnetic fields of 0 T (**b**), 2 T (**c**) and 8 T (**d**). These measurements show diamonds of suppressed conductance shrinking in both the source–drain bias and gate voltage directions with increasing magnetic field.

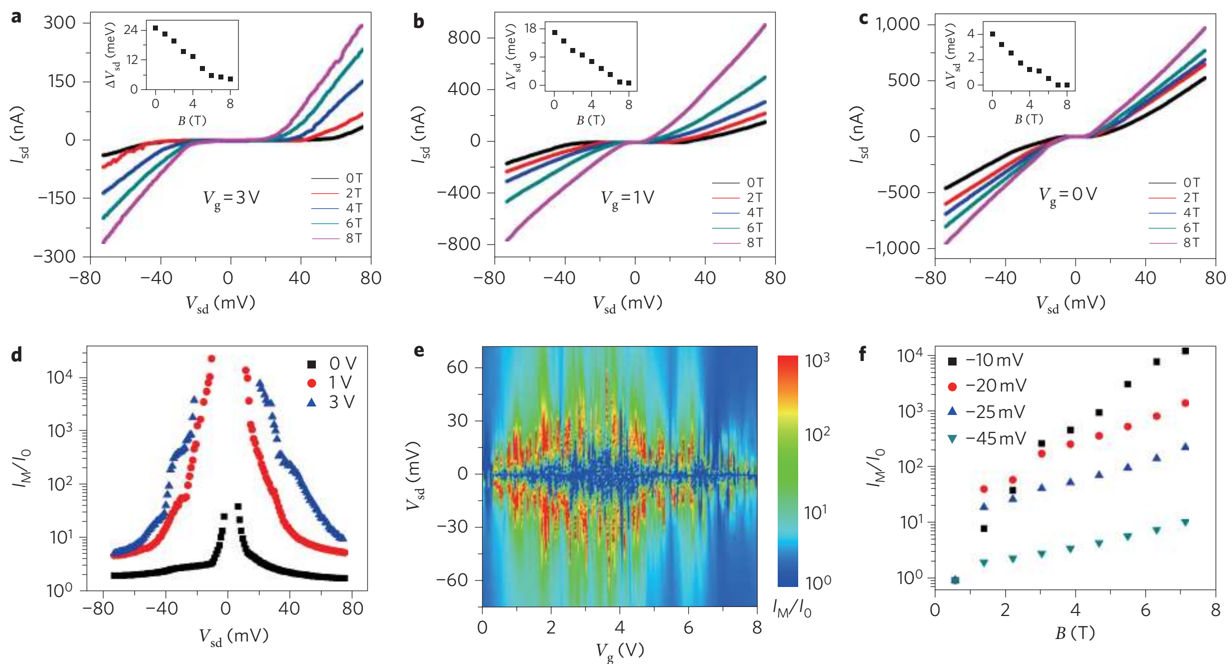

Figure 3 | Tunable magnetoresistance in a graphene nanoribbon FET device. a–c, Impact of magnetic field on current–voltage characteristics when the device is gated at $V = 3$ V (**a**), 1 V (**b**) and 0 V (**c**). Each inset shows the source–drain gap (ΔV_{sd}) as a function of magnetic field. **d**, Current ratio I(8 T)/I(0 T) versus source–drain bias at $V_g = 3$ V. The middle interval for each plot is in the range of suppressed conductance, and is beyond our equipment measurement limits. **e**, Current ratio I(8 T)/I(0 T) as a function of source–drain bias and gate voltage, highlighting the huge increase of current under an applied magnetic field when probing the device close to the diamond of suppressed conductance. **f**, Current ratio I(M)/I(0 T) as a function of magnetic field with a source–drain bias of −10, −20, −25 and −45 mV at $V_g = 1$ V.

Figure 3a shows the current–voltage (I–V) characteristics near the charge neutrality point at different magnetic fields. The I–V curves exhibit nonlinear behaviour near zero source–drain bias, with the semiconductor-like nonlinear gap denoted as the source–drain gap decreasing from 25 meV at 0 T to 4.3 meV at 8 T (Fig. 3a, inset). Note that the source–drain gap is defined by a steep logarithmic increase of current (Supplementary Fig. S1)[23]. These results suggest that the transport barrier decreases with increasing magnetic field[9,23]. At the edge of the transport gap (Fig. 2b, $V_g = 1$ V), where the sub-diamonds of the suppressed conductance nearly disappear at a high magnetic field, the source–drain conduction gap decreases from 16.6 to 0.5 meV (Fig. 3b, inset).

© 2010 Macmillan Publishers Limited. All rights reserved.

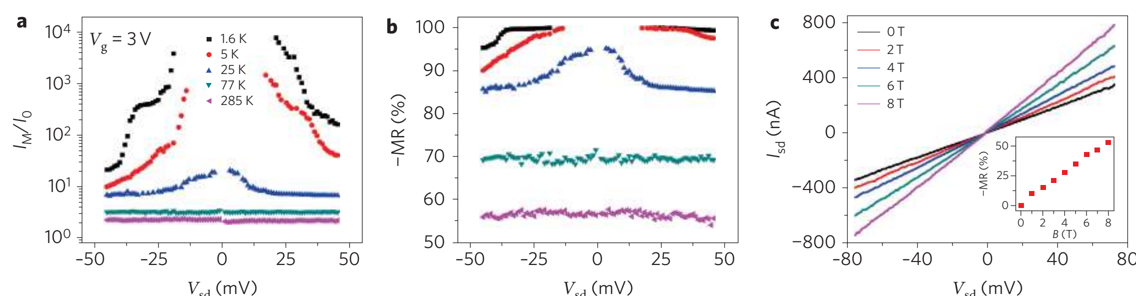

Figure 4 | Temperature-dependent magneto-transport properties. a,**b**, Current ratio I(8 T)/I(0 T) (**a**) and negative magnetoresistance (MR) (**b**) as a function of source–drain bias at 1.6, 5, 25, 77 and 285 K. The device was gated at 3 V. **c**, Room-temperature (285 K) I–V characteristic ($V_g = 3$ V) with different applied magnetic fields. The inset shows the negative magnetoresistance increasing nearly linearly with the applied magnetic field.

Further away from the charge neutrality point ($V_g = 0$ V), the magnetic field has less effect on the device current, although a significant change can still be observed, for example, near zero source–drain bias in the small source–drain gap region, which almost totally disappeared at 8 T (Fig. 3c and inset).

The I–V characteristics indicate that a huge magnetoresistance can be readily obtained by tuning the exact electronic states of the device. Figure 3d plots the current ratio I(8 T)/I(0 T) against source–drain bias at $V_g = 0$, 1 and 3 V. All three curves show a large increase in the current ratio when approaching the transport blockade region. Significantly, an increase in current of over four orders of magnitude can be observed at the edge of the blockade. This exceptionally large magnetoresistance cannot be described accurately using the conventional formula 'magnetoresistance $= \Delta R/R_0$', because a current ratio of over 100 gives a magnetoresistance of −99%, and a change of magnitude by an order of 4 would only give a magnetoresistance value of −99.99%. To better examine the magnitude of the change in conductance, we use the current (conductance) ratio to describe the exceptionally large magnetoresistance in our device. Figure 3d clearly shows that the current ratio can be tuned by a factor of less than 10 to greater than 10,000, depending on the exact gate or source–drain bias. Similar scenarios have also been observed in the electron-transport branch (Supplementary Fig. S2). We have fabricated and studied more than ten devices—all exhibit similar negative magnetoresistance characteristics (Supplementary Figs S3–S5).

Figure 3e provides a general view of the current ratio as a function of both the source–drain bias and gate voltage, further demonstrating the tunability of the magnetoresistance observed in our graphene nanoribbon devices. In general, the current ratio increases significantly when the device is tuned to the proximity of the diamond blockade region, and reaches its highest value at the edge of the conductance suppressing diamond. Within the diamond, the magnetoresistance value could not be accurately determined because the current through the device was below our equipment measurement capability. Figure 3f shows the magnetoresponse at a gate voltage of 1 V and different source–drain bias. In general, the current ratios increase more rapidly with magnetic field when biased closer to the blockade region. In all cases, the current increases exponentially and shows no evidence of saturation up to 8 T (note that the figure has an exponential scale).

Control of magnetoresistance using an electric field has recently attracted considerable attention in multifunctional logic devices. Several material systems, including carbon nanotubes, semiconductor quantum dots and nanowires coupled with ferromagnetic (FM) electrodes, have been explored in this regard, but only limited tunability has been achieved to date[29–31]. Importantly, our studies demonstrate that the graphene nanoribbons themselves, without artificially engineered FM contacts, can exhibit extraordinary magnetoresistance (nearly −100% with a current ratio of over 10,000) that is highly tunable by either varying the gate voltage or source–drain bias, thus enabling an entirely new material system and device structure for multifunctional magnetic logic devices.

We have also studied the evolution of the magnetoresistance with increasing temperature. Figure 4a,b shows the current ratio and negative magnetoresistance versus source–drain bias at different temperatures and $V_g = 3$ V. The maximum current ratio decreases from more than 10,000 at 1.6 K to nearly 20 (magnetoresistance = −95%) at 25 K and 3 (magnetoresistance = −70%) at 77 K, as the conductance suppression due to the conduction bandgap and/or Coulomb blockade effect is weakened with the increase in temperature. The conduction bandgap apparently disappears at room temperature, as the device shows linear transport behaviour (Fig. 4c). At this point, the magnetoresistance can no longer be modified by the source–drain bias voltage, and is only weakly tunable by the gate voltage. Nonetheless, the negative sign of the magnetoresistance persists up to room temperature. A nearly linear increase of magnetoresistance with magnetic field and up to −56% magnetoresistance is obtained at 8 T at $V_g = 3$ V (Fig. 4c, inset). For practical considerations, it is worthwhile noting the magnetoresistance at low magnetic fields. The room-temperature magnetoresistance reaches ~4% at a low magnetic field of 0.5 T, which is not as striking as the low-temperature data (up to 50% at 0.5 T), but it is still very significant in a device that contains no FM materials. It is now well known that the conduction bandgap of graphene nanoribbon is inversely proportional to the ribbon width, and sub-5-nm nanoribbons can develop large enough conduction bandgaps to completely shut off the conductance, even at room temperature[9–11]. Based on our observation of magnetoresistance enhancement near the conductance suppression diamond, a larger magnetoresistance at room temperature may be achievable when the ribbon width is further reduced to the sub-5-nm regime.

To further elucidate the magnetoresistance effect in our device, we fabricated a shorter-channel graphene nanoribbon device with a channel length of 200 nm, aiming to reduce the number of quantum dots along the nanoribbon device[22]. Indeed, simpler transport characteristics with better resolved Coulomb blockade structures were observed in this shorter device (Fig. 5a), although the jointed diamonds still indicated a multiple Coulomb blockade effect[20]. Upon applying magnetic fields of 3 and 6 T, a shrinking of each diamond may be clearly observed (Fig. 5b,c). The size of the diamond structure (bias gap) shrinks consistently with increasing magnetic field (Supplementary Fig. S6). The gate sweeps show an overall conductance increase: the conductance peak grows and broadens and a conductance valley arises, resulting in a diminishing of the blockade region (Fig. 5d). Interestingly, the blockade position is not significantly shifted with magnetic field up to 3 T, indicating no significant change in the quantum dot configuration. These diamonds almost disappear when the magnetic field is increased to 6 T, suggesting that charge hopping through the nanoribbon can be significantly enhanced under an external magnetic field.

© 2010 Macmillan Publishers Limited. All rights reserved.

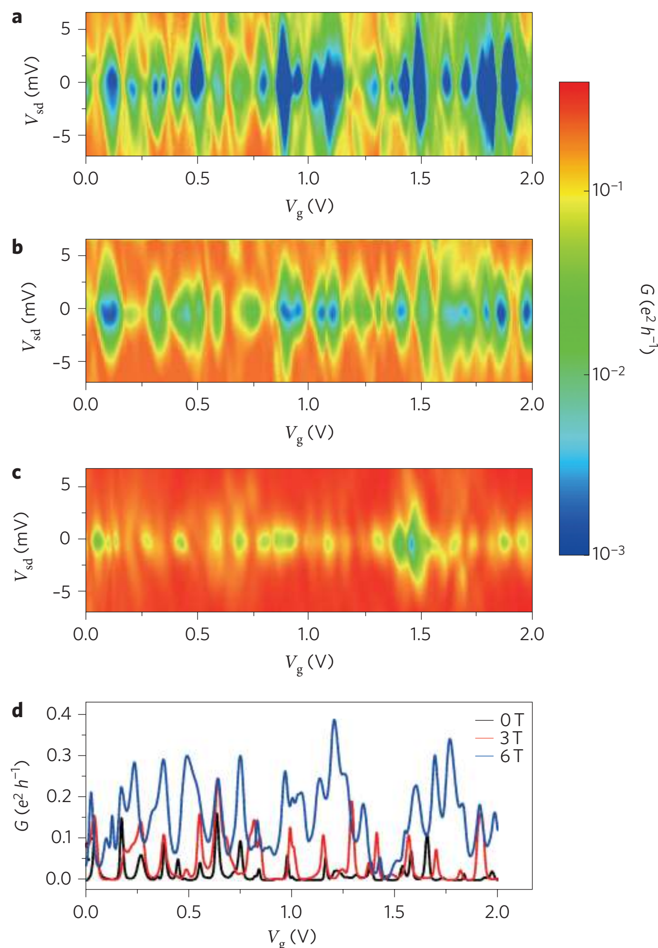

Figure 5 | Magneto-transport properties of a short-channel graphene nanoribbon FET device with a width of 37 nm and length of 200 nm. **a–c**, Differential conductance measurements as a function of source–drain bias and gate voltage at 0 T (**a**), 3 T(**b**) and 6 T (**c**) showing the evolution of the diamonds of suppressed conductance with increasing magnetic field. **d**, Differential conductance G versus gate voltage at zero source–drain bias with an applied magnetic field of 0, 3 and 6 T.

Previous theoretical studies have predicted interesting magneto-transport properties in graphene nanoribbons with multiple possible origins. For example, first-principle calculations have predicted the existence of a semiconducting anti-FM spin state in zigzag graphene nanoribbons that can be excited to the metallic FM state with an applied magnetic field[12–14]. However, this possibility was eliminated in our devices by performing magnetoresistance measurements with an in-plane magnetic field for which no obvious magnetic response was found (Supplementary Fig. S7). On the other hand, recent theoretical studies indicate that a perpendicular magnetic field can greatly modify lateral quantum confinements in graphene nanoribbons and profoundly affect the charge transport due to the formation of cyclotron orbits originating from Dirac–Landau-level behaviour in the graphene nanoribbons[15–20]. It is suggested that a perpendicular magnetic field can induce cyclotron orbits of the electron motion with cyclotron length $l_B = (\hbar/eB)^{1/2}$, where e is the electron charge and B the magnetic field. At lower magnetic fields with large cyclotron length, the cyclotron wavefunction extends beyond the ribbon width, electron motion is strongly affected by the ribbon edges, and the quantum confinement dictates the electrical properties of the graphene nanoribbons. With increasing magnetic field, the cyclotron length decreases. When the cyclotron length becomes comparable to or smaller than the ribbon width, the ribbon edges and confinement potential become less relevant in the ribbon electrical properties, eventually completely eliminating the edge confinement to induce a semiconductor–metal transition at a high enough magnetic field[17–19]. Recent tight-binding calculations have shown that the confinement bandgap of semiconducting armchair graphene nanoribbons indeed shrinks continuously with increasing magnetic field[17]. The cyclotron length is 26.6 nm at 1 T and 9.4 nm at 8 T, comparable to our nanoribbon widths, suggesting that the magnetic field can indeed significantly modify the electronic structure and charge transport in our graphene nanoribbon devices.

In a typical graphene nanoribbon with multi-Coulomb blockade transport characteristics due to experimental edge roughness and local potential variation, the confinement gaps function as energy barriers for charge transport across different electron–hole puddles along the nanoribbon[8,22]. Therefore, a decrease in the confinement gap with magnetic field can reduce the charge hopping barrier in the multi-Coulomb blockade device, and effectively reduce the overall conduction bandgap with increasing magnetic field, as we have observed in our devices (Fig. 3a, inset). This is also consistent with the evolution of the diamond structure in our short-channel device, in which the sizes of the Coulomb diamonds clearly shrink with increasing magnetic field. Our temperature-dependent studies also show that the thermal activation energy of charge transport in the graphene nanoribbons decreases with increasing magnetic field, further suggesting shrinking of the confinement gaps[31] by the perpendicular magnetic field (Supplementary Fig. S8). Additionally, the edge roughness induced back-scattering, in terms of strong localization, may also contribute to the observed conductance suppression[6], in which the magnetic field can induce the delocalization effect, suppress the back-scattering, and therefore enhance the conductance[32]. The Coulomb blockade effect can significantly enhance the magnetoresistance at the edge of the transport gap/source–drain gap, where charge transport is more sensitive to the magnetic field. On the other hand, when gated or biased outside the transport gap or under high temperature, where current flow is dominated by drifting and the conductance is limited by edge or charge impurity scattering, the observed magnetoresistance is expectedly not as striking as that under tunnelling conditions.

In conclusion, we have reported an extraordinarily large tunable magnetoresistance in graphene nanoribbon–FET devices. A negative magnetoresistance of nearly 100% with an increase in conductance by a factor of over 10,000 was demonstrated at 1.6 K, and a negative magnetoresistance of nearly 56% was obtained at room temperature. This magnetoresistance can be readily tuned by the gate voltage and source–drain bias, with enhancement reaching maxima near the edges of the conduction bandgap. Although further experimental and theoretical studies will be necessary to fully elucidate the exact mechanism responsible for the observed negative magnetoresistance, our experimental findings clearly demonstrate that the graphene nanoribbons exhibit interesting magneto-transport properties, with the possibility of opening up exciting opportunities in magnetic sensing and a new generation of magneto-electronic devices.

During manuscript revision and the editorial process, we have become aware of preprints on similar topics posted on condensed matter arXiv[33,34]. Our work was developed independently from the work reported in these preprints.

Methods

The graphene nanoribbon–FETs were fabricated using SiO_2 nanowires as the physical etching masks[11]. Silicon nanowires with diameters ranging from 5 to 40 nm were grown using a catalytic chemical vapour deposition, and oxidized in air at 900 °C for 15 min to produce an SiO_2 insulating shell or fully oxidized nanowires. Graphene flakes were mechanical peeled from natural graphite onto heavily doped p-type silicon wafers with a 300-nm layer of thermal oxide. The SiO_2 nanowires were

© 2010 Macmillan Publishers Limited. All rights reserved.

then physically transferred from the growth substrate to the graphene substrate using a contact printing approach. Specifically, a graphene device substrate was first firmly attached to a benchtop, and the nanowire substrate placed upside down on top of the graphene device substrate so that the nanowires were in contact with the graphene. A gentle manual pressure was then applied from the top, followed by slightly sliding the growth substrate. The nanowires were transferred onto the graphene device substrate by shear forces during the sliding process. The sample was then rinsed with isopropanol, then blown dry using nitrogen, with the capillary drying process near the nanowires helping them to become firmly attached to the graphene flakes. The nanowire position was determined by dark-field microscopy or atomic force microscopy. Electron-beam lithography was used to define the source and drain electrodes according to the position of the nanowires on the graphene, and a titanium/gold (7 nm/90 nm) film was evaporated with an electron-beam evaporator. The graphene regions not protected by the nanowires were etched away by oxygen plasma under 30–40 W for 20 s. Transport measurements were carried out in a pumped liquid-helium system equipped with a superconducting magnet (American Magnetics). Differential conductance (dI/dV) measurements were performed using a standard lock-in detection technique in which a superimposed low-frequency (17 Hz) a.c. current modulation was measured as a function of a d.c. voltage bias component.

Received 4 May 2010; accepted 25 June 2010;
published online 8 August 2010

References

1. Geim, A. K. & Novoselov, K. S. The rise of graphene. *Nature Mater.* **6,** 183–191 (2007).
2. Castro Neto, A. H., Guinea, F., Peres, N. M. R., Novoselov, K. S. & Geim, A. K. The electronic properties of graphene. *Rev. Mod. Phys.* **81,** 109–162 (2009)
3. Nakada, K., Fujita, M., Dresselhaus, G. & Dresselhaus, M. S. Edge state in graphene ribbons: nanometer size effect and edge shape dependence. *Phys. Rev. B* **54,** 17954–17961 (1996).
4. Son, Y. W., Cohen, M. L. & Louie, S. G. Energy gaps in graphene nanoribbons. *Phys. Rev. Lett.* **97,** 216803 (2006).
5. Sols, F., Guinea, F. & Neto, A. H. C. Coulomb blockade in graphene nanoribbons. *Phys. Rev. Lett.* **99,** 166803 (2007).
6. Gunlycke, D., Areshkin, D. A. & White, C. T. Semiconducting graphene nanostrips with edge disorder. *Appl. Phys. Lett.* **90,** 142104 (2007).
7. Adam, S., Cho, S., Fuhrer, M. S. & Das Sarma, S. Density inhomogeneity driven percolation metal–insulator transition and dimensional crossover in graphene nanoribbons. *Phys. Rev. Lett.* **101,** 046404 (2008).
8. Stampfer, C. *et al.* Energy gaps in etched graphene nanoribbons. *Phys. Rev. Lett.* **102,** 056403 (2009).
9. Han, M. Y., Ozyilmaz, B., Zhang, Y. B. & Kim, P. Energy bandgap engineering of graphene nanoribbons. *Phys. Rev. Lett.* **98,** 206805 (2007).
10. Li, X. L., Wang, X. R., Zhang, L., Lee, S. W. & Dai, H. J. Chemically derived, ultrasmooth graphene nanoribbon semiconductors. *Science* **319,** 1229–1232 (2008).
11. Bai, J. W., Duan, X. F. & Huang, Y. Rational fabrication of graphene nanoribbons using a nanowire etch mask. *Nano. Lett.* **9,** 2083–2087 (2009).
12. Son, Y. W., Cohen, M. L. & Louie, S. G. Half-metallic graphene nanoribbons. *Nature* **444,** 347–349 (2006).
13. Kim, W. Y. & Kim, K. S. Prediction of very large values of magnetoresistance in a graphene nanoribbon device. *Nature Nanotech.* **3,** 408–412 (2008).
14. Munoz-Rojas, F., Fernandez-Rossier, J. & Palacios, J. J. Giant magnetoresistance in ultrasmall graphene based devices. *Phys. Rev. Lett.* **102,** 136810 (2009).
15. Peres, N. M. R., Castro Neto, A. H. & Guinea, F. Dirac fermion confinement in graphene. *Phys. Rev. B* **73,** 241403 (2006).
16. Peres, N. M. R., Castro Neto, A. H. & Guinea, F. Conductance quantization in mesoscopic graphene. *Phys. Rev. B* **73,** 195411 (2006).
17. Huang, Y., Chang, C. P. & Lin, M. F. Magnetic and quantum confinement effects on electronic and optical properties of graphene ribbons. *Nanotechnology* **18,** 495401 (2007).
18. Liu, J., Wright, A. R., Zhang, C. & Ma, Z. Strong terahertz conductance of graphene nanoribbons under a magnetic field. *Appl. Phys. Lett.* **93,** 041106 (2008).
19. Ritter, C., Makler, S. S. & Latge, A. Energy-gap modulations of graphene ribbons under external fields: a theoretical study. *Phys. Rev. B* **77,** 195443 (2008).
20. Li, T. S., Huang, Y. C., Chang, S. C., Chang, C. P. & Lin, M. F. Magnetoconductance of graphene nanoribbons. *Phil. Mag.* **89,** 697–709 (2009).
21. Lin, Y. M., Perebeinos, V., Chen, Z. H. & Avouris, P. Electrical observation of subband formation in graphene nanoribbons. *Phys. Rev. B* **78,** 161409 (2008).
22. Gallagher, P., Todd, K. & Foldhaber-Gordon, D. Disorder-induced gap behavior in graphene nanoribbons. *Phys. Rev. B* **81,** 115409 (2010).
23. Han, M. Y., Brant, J. C. & Kim, P. Electron transport in disordered graphene nanoribbons. *Phys. Rev. Lett.* **104,** 056801 (2010).
24. Ozyilmaz, B., Jarillo-Herrero, P., Efetov, D. & Kim, P. Electronic transport in locally gated graphene nanoconstrictions. *Appl. Phys. Lett.* **91,** 192107 (2007).
25. Scott Bunch, J. S., Yaish, Y., Brink, M., Bolotin, K. & McEuen, P. L. Coulomb osillations and Hall effect in quasi-2D graphite quantum dots. *Nano Lett.* **5,** 287–290 (2005).
26. Ponomarenko, L. A. *et al.* Chaotic Dirac billiard in graphene quantum dots. *Science* **320,** 356–358 (2008).
27. Cho, S. & Fuhrer, M. S. Charge transport and inhomogeneity near the minimum conductivity point in graphene. *Phys. Rev. B* **77,** 081402 (2008).
28. Martin, J. *et al.* Observation of electron–hole puddles in graphene using a scanning single-electron transistor. *Nature Phys.* **4,** 144–148 (2008).
29. Sahoo, S. *et al.* Electric field control of spin transport. *Nature Phys.* **1,** 99–102 (2005).
30. Hamaya, K. *et al.* Electric-field control of tunneling magnetoresistance effect in a Ni/InAs/Ni quantum-dot spin valve. *Appl. Phys. Lett.* **91,** 022107 (2007).
31. Martin, I. & Blanter, Y. M. Transport in disordered graphene nanoribbons. *Phys. Rev. B* **79,** 235132 (2009).
32. Gershenson, M. E., Khavin, Y. B., Mikhalchuk, A. G., Bozler, H. M. & Bogdanov, A. L. Crossover from weak to strong localization in quasi-one-dimensional conductors. *Phys. Rev. Lett.* **79,** 725–728 (1997).
33. Poumirol, J. M. *et al.* Edge magneto-fingerprints in disordered graphene nanoribbons. Preprint at arXiv: 1002.4571v1 (2010).
34. Oostinga, J. B., Sacepe, B., Cracium, M. F. & Morpurgo, A. F. Magneto-transport through graphene nanoribbons. Preprint at arXiv: 1003.2994v1 (2010).

Acknowledgements

The authors would like to acknowledge technical support from the Center for Quantum Research and the Nanoelectronics Research Facility at UCLA. The authors thank D. Newhauser and Y. Tserkovnyak for discussions. Y.H. acknowledges support from the Henry Samueli School of Engineering and an Applied Science Fellowship. X.D. acknowledges support from NSF CAREER award 0956171 and the NIH Director's New Innovator Award Program, part of the NIH Roadmap for Medical Research, through grant no. 1DP2OD004342-01.

Author contributions

X.D., Y.H., J.B., R.C. and L.L. conceived and designed the experiments. J.B., C.R., F.X. and A.S. performed the experiments. J.B. and C.R. collected and analysed the data. M.W., A.S. and K.W. contributed experimental tools. J.B., C.R., Y.H. and X.D. co-wrote the paper. All authors discussed the results and commented on the manuscript.

Additional information

The authors declare no competing financial interests. Supplementary information accompanies this paper at www.nature.com/naturenanotechnology. Reprints and permission information is available online at http://npg.nature.com/reprintsandpermissions/. Correspondence and requests for materials should be addressed to X.D. and Y.H.

© 2010 Macmillan Publishers Limited. All rights reserved.